(Received 25 November 2025, Accepted 9 January 2025, Scheduled 18 January 2025)

Design of a Compact Wideband Filtering Antenna with High Frequency Selectivity

Hao Gui[1], Zhonggen Wang[1], Wenyan Nie[2,*], Ming Yang[3], and Mingqing Wang[1]

[1]*School of Electrical and Information Engineering, Anhui University of Science and Technology, Huainan 232001, China*
[2]*School of Mechanical and Electrical Engineering, Huainan Normal University, Huainan 232001, China*
[3]*School of Electrical and Communications Engineering, West Anhui University, Lu'an 237012, China*

ABSTRACT: A low-profile monolayer filtering antenna with compact size is presented in this paper. The antenna features a simple structure, comprising a substrate, a stepped defective ground structure, an asymmetric Y-shaped branch, and a microstrip feedline with an L-shaped branch. The asymmetric Y-shaped branch and L-shaped branch feedline collaborate to introduce two additional resonant frequency points, thereby broadening the impedance bandwidth. Furthermore, two radiation nulls are introduced on either side of the passband, which enhances the frequency selectivity of the band edges and optimizes the antenna's radiating and filtering performances. To verify the proposed design, a prototype of the compact filtering antenna was fabricated and measured. The measured and simulated results show good agreement. The design achieves a wide impedance bandwidth of 44.6% (4.88 $\sim$ 7.68 GHz) at a center frequency of 6.22 GHz, a peak realized gain of 5.7 dBi, and a compact size of 35 mm$\times$29 mm$\times$0.8 mm. Two radiation nulls on either side of the passband result in an excellent band-pass response, with out-of-band rejection reaching 18.2 dB. Finally, the antenna's excellent radiation performance and filtering characteristics make it suitable for wireless communication applications in the 5G Sub-6 GHz and WiFi-6E bands.

1. INTRODUCTION

With the rapid advancement of wireless communication technology, radio frequency (RF) equipment is increasingly characterized by multifunctionality, integration, and miniaturization. In wireless communication systems, antennas and filters, serving as critical components of RF front-ends, are responsible for transmitting and receiving signals while filtering out interference. Traditionally, antennas need to be cascaded with additional filter elements to achieve band-pass filtering. Recently, filtering antennas, which combine the filtering capabilities of filters with the radiation characteristics of antennas, have emerged as an effective solution. This approach reduces the size of RF devices and incorporate additional functionalities without compromising antenna performance, thereby enhancing circuit integration.

In conventional filtering antenna design methods, antenna and filter [1] are designed independently and then cascaded using transmission lines [2, 3], or the final resonator of a multi-resonator coupled bandpass filter is utilized as the radiating element [4–8]. In [1], a miniaturized filtering power divider comprising a coupled microstrip line with three resonators was presented to achieving a tri-band filtering response. In [8], a composite right/left-handed transmission line (CRLH-TL) resonator serves as the filter element; an L-shaped patch acts as the radiating element; and an asymmetric coplanar waveguide (CPW) feeding [9] achieves a passband flat gain of 2.5 dBi and an impedance bandwidth of 23.5%. Notably, the co-design of antennas and filters has been introduced to create filtering antennas that can simultaneously receive/transmit and filter electromagnetic waves. As presented in [10], a dielectric resonator antenna with a quadrature coupler was developed. It features a snowflake-shaped patch and achieves a wide impedance bandwidth of 27.8%. This design also provides superior band-pass filtering and extensive harmonic suppression. However, it is complex to configure and incurs high manufacturing costs.

Although these methods can achieve both the antenna's radiation performance and the filter's filtering capabilities, they increase the overall size and complexity of the device. As a result, they lead to higher insertion losses and are not conducive to miniaturization. In recent years, the primary approach for filtering antenna design has been the integration of antenna and filter functionalities. This integrated design is realized through techniques such as introducing slot-loaded patches [11–14], adding parasitic patches [15–19], utilizing shorted vias [20, 21], employing defected ground structures (DGS) [22–24], combining metasurface antenna structures [25, 26], and using stacked patches [19, 21, 27–29] to generate radiation nulls near the operational band. In [11], a filtering slot antenna design was proposed to generate three out-of-band radiation nulls by manipulating the hybrid electric and magnetic coupling between the slots, resulting in a broadband filtering slit antenna with three slits. The compact slit antenna achieves an impedance bandwidth of 33.8%, but its peak gain is relatively low at 4.1 dBi, and the out-of-band rejection is limited to 12.1 dB, indicating room for further optimization. In [18], a low-profile single-layer filtering antenna was developed using a short-circuited parasitic patch and a folded defected ground structure to create radiation nulls on both sides of

* Corresponding author: Wenyan Nie (wynie5240@163.com).

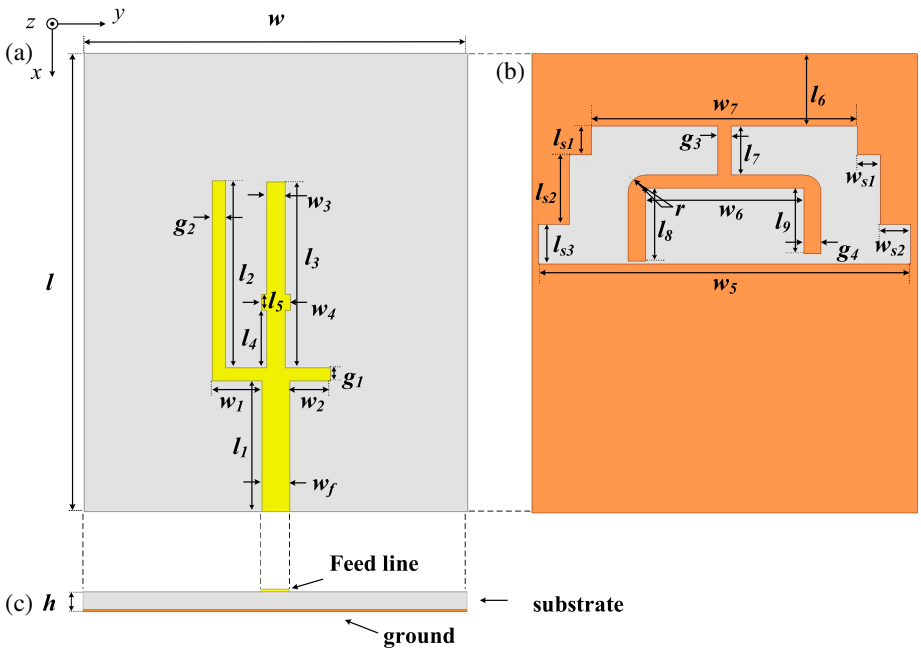

FIGURE 1. Configuration of the proposed filtering antenna. (a) Top view. (b) Bottom view. (c) Side view.

the passband, thereby achieving a filtering effect. However, it only achieves an impedance bandwidth of 9.2% and an out-of-band rejection of 11 dB, which is somewhat limited in performance. In [26], two novel dual-polarization filtering metasurface antennas were introduced, featuring uniformly distributed square metasurface structures combined with polarized cross-slots. By incorporating short truncation lines and etched slots into the metasurface structures, radiation nulls are generated on both sides of the passband, achieving an out-of-band rejection exceeding 30 dB. However, this design exhibits reduced radiation performance and involves a complex fabrication process. In [28], a stacked circularly polarized filtering patch antenna with controllable radiation nulls was developed, utilizing etched slots on the upper and lower patches to achieve the filtering effect. However, this stacked patch design features a relatively complex structure and a narrow impedance bandwidth. Therefore, achieving an optimal balance among a simple compact structure, wide bandwidth, and robust radiation performance remains a significant challenge for filtering antennas using integrated design approaches.

Compared to the traditional cascade approach, this integrated design method minimizes both losses and the overall system size by eliminating the need for a separate filter structure, thereby achieving superior filtering performance without compromising antenna gain. Additionally, optimal filtering performance can be achieved by employing a multilayer structure [25, 28] or by fine-tuning specific structural parameters to control bandwidth and adjust the positioning of radiation nulls. Based on this design concept, this paper proposes a single-layer broadband filtering antenna featuring a compact size, wide bandwidth, high frequency selectivity, and flat gain, utilizing a single-port microstrip-fed structure. The introduction of a Y-shaped branch on the stepped defected ground plane generates two radiation nulls in the gain response on either side of the passband, resulting in enhanced band-pass characteristics and improved out-of-band rejection level. Furthermore, an L-shaped branch is added on the substrate's top surface to generate additional resonant points. This broadens the operating bandwidth and enhances the frequency selectivity of high-frequency radiation null, achieving a superior filtering effect. Finally, to thoroughly analyze and validate the antenna's radiation and filtering capabilities, a prototype was fabricated and measured, focusing on the mechanisms behind radiation null generation and the impact of various design parameters. Measurement results indicate that the proposed antenna, with dimensions of 35 mm×29 mm×0.8 mm, achieves an impedance bandwidth of 44.6% (4.88∼7.68 GHz) at a standard return loss of 10 dB, along with a peak gain of 5.7 dBi and an out-of-band rejection level of 18.2 dB. These findings demonstrate excellent in-band radiation and robust out-of-band rejection, confirming the antenna's superior radiation and filtering performance. In complex communication scenarios, the proposed antenna effectively covers the 5G Sub-6 GHz band (n77, n78, and part of n79) as well as the WiFi-6E band, rendering it highly suitable for small base stations, high-speed wireless routers, industrial Internet of Things (IoT), and wireless AR/VR devices. Furthermore, similar to the circularly polarized antenna used in [30] for Dedicated Short-Range Communication (DSRC) systems, the proposed antenna can also support short-range communications within the ISM band (5.8 GHz), including wireless sensor networks and indoor positioning.

2. ANTENNA DESIGN

2.1. Antenna Configuration

The overall structure of the proposed filtering antenna is depicted in Figure 1. The antenna is printed on a single dielectric substrate and includes a stepped defective rectangular ground

TABLE 1. Dimensions of filtering antenna: (mm).

Parameter	l	l_1	l_2	l_3	l_4	l_5	l_6	l_7	l_8	l_9
Value	35	10	14.3	14.2	4.4	1.2	5.5	3.75	5.55	5
Parameter	h	w	w_f	w_1	w_2	w_3	w_4	w_5	w_6	w_7
Value	0.8	29	2.1	3.75	3.1	1.4	2.2	28	11.9	20
Parameter	l_{s1}	l_{s2}	l_{s3}	w_{s1}	w_{s2}	g_1	g_2	g_3	g_4	r
Value	2.2	5.3	3	1.7	2.3	1	1	1	1.3	1.25

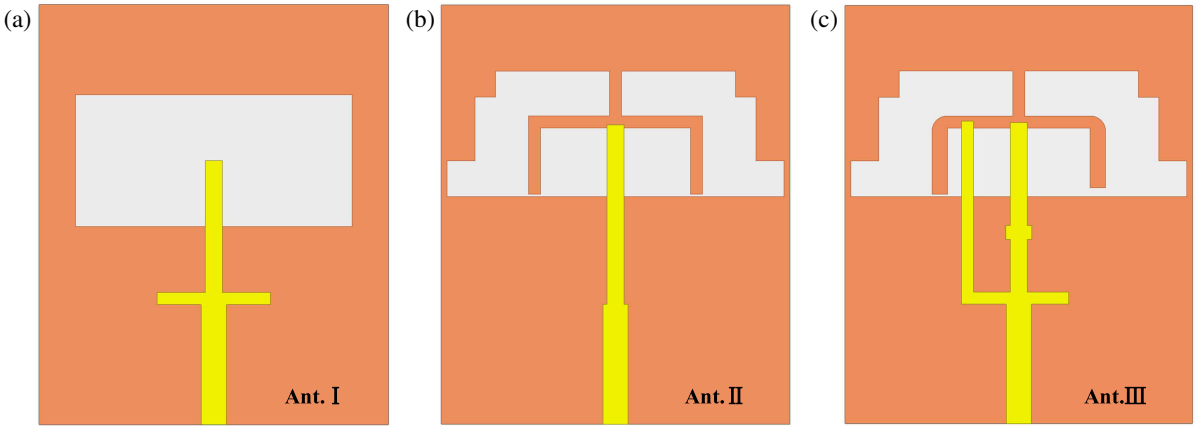

FIGURE 2. Evolution of the proposed filtering antenna. (a) Reference antenna I. (b) Reference antenna II. (c) Proposed antenna III.

plane, a Y-shaped branch, and an asymmetrical microstrip feedline. The dielectric substrate used in this design is FR-4, characterized by a relative permittivity (ε_r) of 4.4, a loss tangent (tanδ) of 0.02, with dimensions of 35 mm×29 mm×0.8 mm. The microstrip feedline is located on the upper surface of the dielectric substrate, consisting of a main branch and an L-shaped branch positioned at two-fifths of the main branch length, forming the complete microstrip feedline. The ground plane on the underside of the dielectric substrate includes a symmetrical stepped defect slot and an asymmetrical Y-shaped branch. The Y-shaped branch is symmetrically positioned at the center of both the substrate and the defect slot, connected directly to the ground plane. The microstrip feedline primarily serves to expand the antenna's impedance bandwidth. Together with the Y-shaped branch and defected ground structure, it generates two radiation nulls at low and high frequencies, thereby improving out-of-band rejection and optimizing the filtering performance. The detailed parameters of the optimized antenna are provided in Table 1.

2.2. Antenna Design Process

To comprehensively explain the design process and filtering mechanism of the proposed antenna, its evolution is illustrated in Figure 2. The initial structure begins with reference antenna I (Ant. I), which is a conventional rectangular wide-slit antenna featuring a rectangular defected ground plane and a crossed microstrip feedline. Reference antenna II (Ant. II) is derived from Ant. I by modifying the crossed microstrip line, transforming the rectangular defected ground plane into a stepped shape, and introducing a symmetrical Y-shaped branch. The proposed antenna III (Ant. III) is developed by further refining the microstrip feed line and Y-shaped branch based on the configurations of Ant. I and Ant. II. In Ant. III, the microstrip feedline comprises a main branch and an additional L-shaped branch, while the ground plane features an asymmetric Y-shaped branch and a stepped wide slot.

Figure 3 presents the simulated S-parameters and realized gains for both reference antennas as well as the proposed antenna. As shown in Figure 3(a), Ant. I exhibits a single resonance point, operating at 6.4 GHz with an impedance bandwidth of approximately 10.8% (6.02∼6.71 GHz). Meanwhile, Figure 3(b) indicates a peak gain of 5.4 dBi for Ant. I However, it suffers from poor out-of-band rejection and lacks significant filtering performance.

Ant. II exhibits two distinct resonance points. Modifications to the ground plane improve impedance matching and expand the antenna's operational bandwidth. Additionally, the introduction of a symmetrical Y-shaped branch creates a new resonance point in the low-frequency band, thereby extending the impedance bandwidth by approximately 27.1% (5.13∼6.74 GHz). Figure 3(b) further illustrates the presence of two radiation nulls, f_{n1} and f_{n2}, in the gain response of Ant. II at 3.82 GHz and 8.74 GHz, respectively. In this configuration, the gain of Ant. II sharply drops from 5.4 dBi to −28.8 dBi, producing radiation nulls on both sides of the passband, thereby achieving a more pronounced filtering effect. However, the frequency selectivity in the upper stopband remains insufficient.

Finally, by leveraging the advantages of Ant. I and Ant. II, the proposed antenna (Ant. III) is developed, successfully achiev-

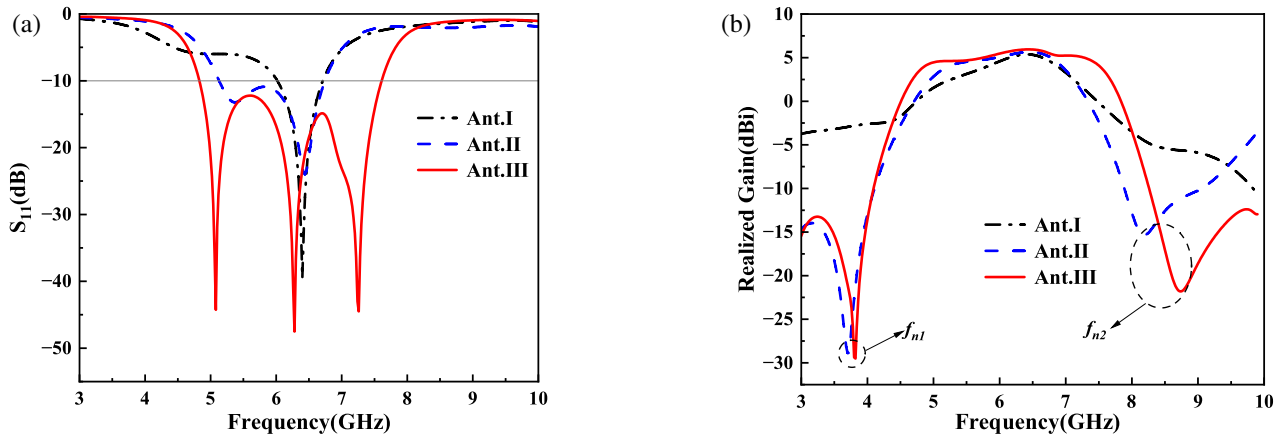

FIGURE 3. The S_{11} and realized gain of the reference antenna and proposed antenna (a) S_{11}. (b) Realized gains.

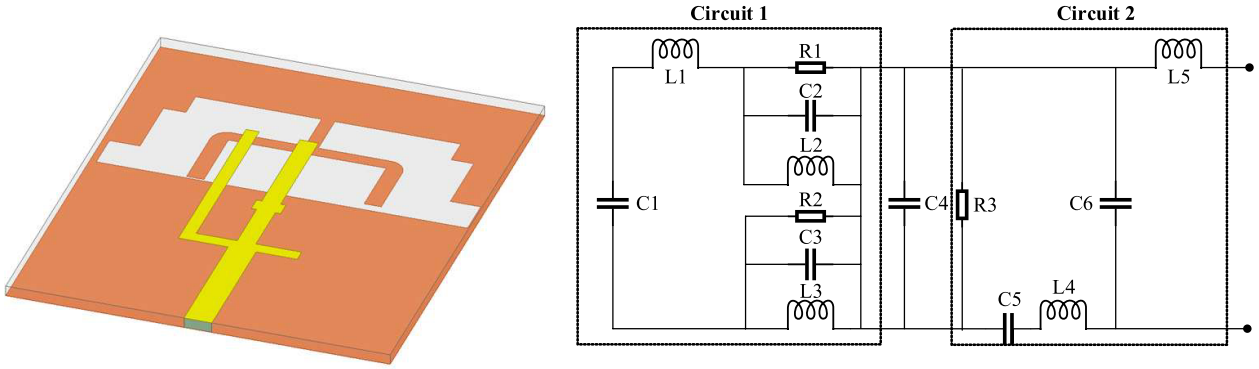

FIGURE 4. Equivalent circuit of the proposed filtering antenna.

ing three resonance points and two radiation nulls. Ant. III represents the finalized design of the proposed antenna. As shown in Figure 3(b), Ant. III achieves a -10 dB impedance bandwidth of approximately 44.7% (4.83∼7.61 GHz) based on the -10 dB return loss criterion, with an average gain around 5.25 dBi and a relatively flat realized gain across the passband. As shown in Figure 3(a), the inclusion of an L-shaped branch at the top of the microstrip feedline in Ant. II introduces a third resonance point (7.26 GHz), significantly expanding the impedance bandwidth while further enhancing frequency selectivity in the upper stopband. The dimensions of the L-shaped branch can be calculated using the following formula:

$$L = l_2 + w_1 + w_f + w_2 \tag{1}$$

$$f_c = \frac{c}{L \times \sqrt{\frac{\varepsilon_r+1}{2}}} \tag{2}$$

where c is the speed of electromagnetic waves, f_c the resonant frequency of 7.26 GHz, and L the effective length of the L-shaped branch. Similarly, the second resonance point can be calculated based on the effective length of the main branch. Specifically, the first low-frequency resonance point and second central resonance point are generated by the main branch of the microstrip feedline and Y-shaped branch, while the third high-frequency resonance point is attributed to the L-shaped branch. A square patch is incorporated into the main branch to enhance impedance matching at high-frequency resonance point, thereby improving overall bandwidth. Compared to Ant. I, the proposed Ant. III significantly broadens the impedance bandwidth. It also achieves superior frequency selectivity by generating two radiation nulls at both the upper and lower passband edges, resulting in excellent radiation and filtering performance. This design eliminates the need for external filters or additional filtering components. It also maintains the antenna size, effectively addressing the miniaturization requirements of RF front-end devices in modern wireless communication systems.

Figure 4 illustrates the equivalent circuit of the proposed antenna, where Circuit 1 is formed by the asymmetrical Y-branch, and Circuit 2 is constituted by the main and L-branch. The Y-branch in the proposed antenna plays a crucial role in generating the filtered response, leading to the formation of two distinct radiation nulls. Capacitor C4 represents the coupling capacitance between the L-shaped branch and the ground plane, playing a critical role in optimizing the filter response for enhanced filter performance.

To evaluate the filtering performance of the proposed antenna, analyzing the radiation nulls is crucial. Figure 5 illustrates the current vector distribution of the final antenna, which is used to further analyze the generation mechanism of the two radiation nulls, f_{n1} at 3.82 GHz and f_{n2} at 8.74 GHz. The current vector distribution for the low-frequency radiation null f_{n1}

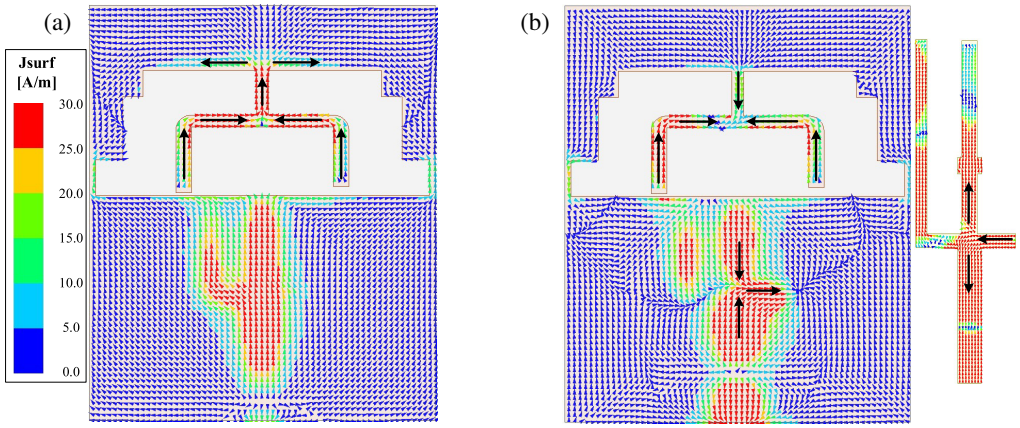

FIGURE 5. Current distribution of the proposed antenna at (a) the radiation null f_{n1} and (b) the radiation null f_{n2}.

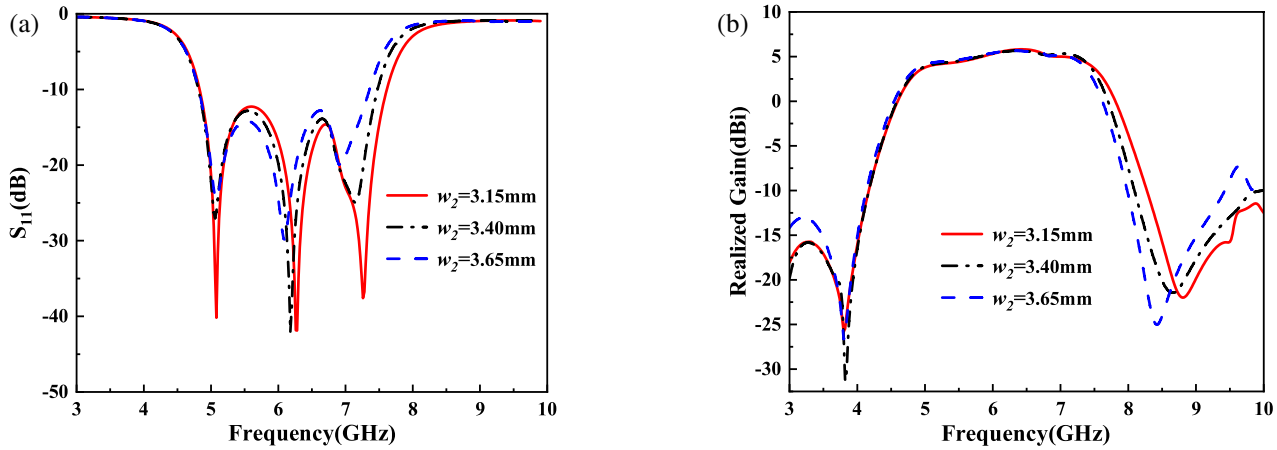

FIGURE 6. Performance of the filtering antenna for different lengths of w_2.

is depicted in Figure 5(a). It is evident that the current is primarily concentrated on the Y-shaped branch. Additionally, the currents on the two branches flow in opposite directions. Consequently, the radiation produced by these opposing currents cancels out, leading to the formation of the low-frequency radiation null f_{n1}. The total length of the Y-shaped branch is approximately one-quarter of the wavelength corresponding to f_{n1}, which can be calculated using the following equation [15]:

$$w_6 + l_8 + l_9 = \lambda_{n1}/4 \tag{3}$$

where λ_{n1} represents the wavelength at f_{n1}. Figure 5(b) shows that at f_{n2}, the currents are primarily concentrated on the Y-shaped branch and external ground plane. A closer examination reveals that the currents on the left and right branches of the Y-shape, along with the inflowing current from the external ground, cancel each other out. Additionally, the currents on the external ground plane flow in opposite directions along the x-axis and are also opposite to the currents in the microstrip line above, resulting in radiation cancellation and enhancing the frequency selectivity of f_{n2}. Thus, f_{n2} is produced by the opposing currents generated within the Y-shaped branch, and between the Y-shaped branch and the external ground, as well as between the microstrip feedline and external ground. The external ground induces a current reversal at the center of the cross-shaped microstrip feedline.

In conclusion, the analysis of the current distribution indicates that radiation cancellation due to current reversal is the primary mechanism behind f_{n1} and f_{n2}.

2.3. Parametric Study

In order to further optimize the antenna performance, certain parameters were analyzed and investigated. The results indicate that the filtering performance of the proposed antenna depends on the lengths of the Y-branch (w_6) and the transverse branch of the microstrip line (w_2). Subsequently, a detailed analysis of parameters w_6 and w_2 helps to better understand the mechanism behind the generation of radiation nulls in the filtering antenna. Figure 6 presents the simulated realized gains and reflection coefficients as the lengths of w_6 and w_2 are varied. As depicted in Figure 6(a), increasing the length of w_2 from 3.15 mm to 3.65 mm shifts the center resonance frequency down from 6.28 GHz to 6.08 GHz. The third resonance frequency decreases from 7.26 GHz to 6.92 GHz, while the low-frequency resonance point remains nearly unchanged. It is evident that the length of w_2 primarily influences the two high-frequency resonance points. As w_2 increases, the antenna's op-

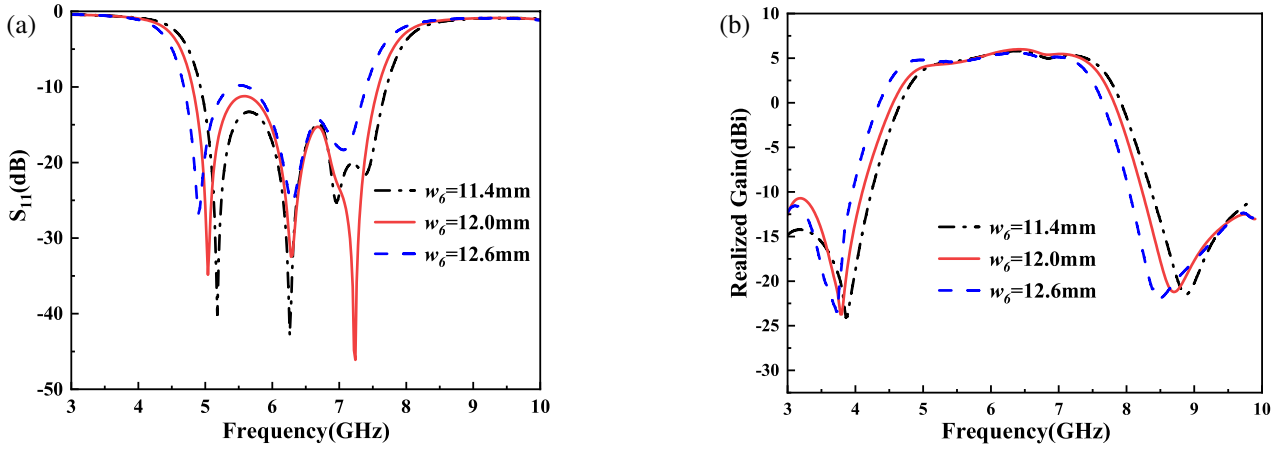

FIGURE 7. Performance of the filtering antenna for different lengths of w_6.

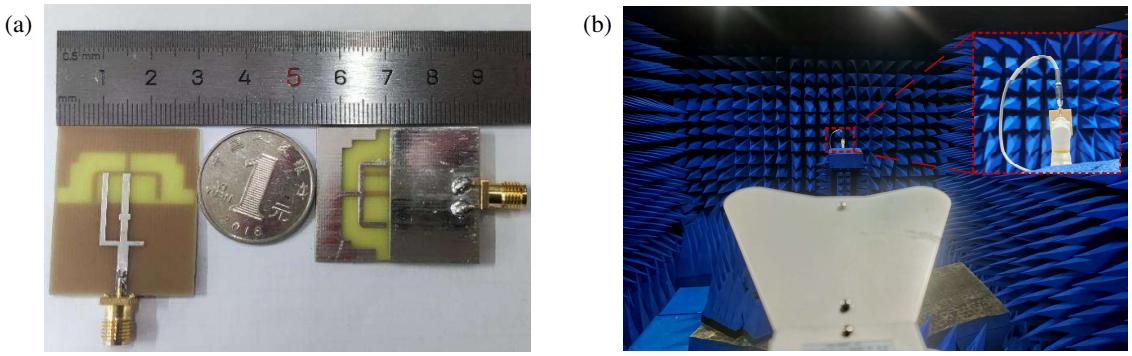

FIGURE 8. Photographs of (a) the fabricated antenna and (b) the measurement environment.

erational bandwidth narrows, and impedance matching deteriorates. Figure 6(b) illustrates that increasing w_2 shifts the high-frequency radiation null towards lower frequencies, while the other null remains largely unaffected. Thus, the high-frequency radiation null is primarily influenced by the length of w_2, allowing for independent control of its position by adjusting w_2.

Similarly, Figure 7 presents the results for varying lengths of the Y-branch. As illustrated in Figure 7(a), increasing the length of w_6 shifts the overall operating frequency of the antenna to a lower band, while the central resonance point remains relatively stable. Simultaneously, Figure 7(b) shows that the two radiation nulls, f_{n1} and f_{n2}, also shift synchronously to lower frequencies. Thus, adjusting w_6 can impact both the operating frequency range and the positions of the two radiation nulls. Finally, parametric studies indicate that altering the lengths of w_2 and w_6 allows for control over the two radiation nulls at the passband edges, thereby achieving the desired filtering effect.

3. MEASUREMENT AND COMPARISON

3.1. Antenna Model Measurement

The proposed filtering antenna was designed and simulated using HFSS electromagnetic simulation software. For experimental validation, the antenna was fabricated, with SMA coaxial connectors soldered to the end of the microstrip feed line. The fabricated compact broadband filtering antenna is depicted in Figure 8(a). The S-parameters and radiation characteristics were measured using an AV3629D vector network analyzer and the microwave radio darkroom, as illustrated in Figure 8(b).

Figure 9 presents the simulated and measured S-parameters, realized gains, and radiation efficiencies of the proposed antenna. The simulated and measured S-parameters show good agreement. These results exhibit -10 dB impedance bandwidths of 44.7% (4.83∼7.61 GHz) and 44.6% (4.88∼7.68 GHz), respectively, which clearly demonstrates the presence of three resonance points. The gain profile of the antenna remains relatively flat within the passband. The simulated and measured peak realized gains are 6.0 dBi and 5.7 dBi, respectively, both of which decline sharply outside the passband, indicating the antenna's effective filtering characteristics. Additionally, two radiation nulls are observed on both sides of the passband at 3.82 GHz (3.72 GHz) and 8.74 GHz (8.82 GHz). These nulls result in significant gain rejection levels of 19.22 dB (19.1 dB) at the lower edge and 18.35 dB (18.2 dB) at the upper edge. Furthermore, the simulated radiation efficiency exceeds 85%, with the two nulls clearly visible in the antenna efficiency curve, highlighting the antenna's high efficiency, low loss, and high selectivity. Figure 10 presents the simulated and measured results of the E-plane and H-plane radiation patterns at three resonance

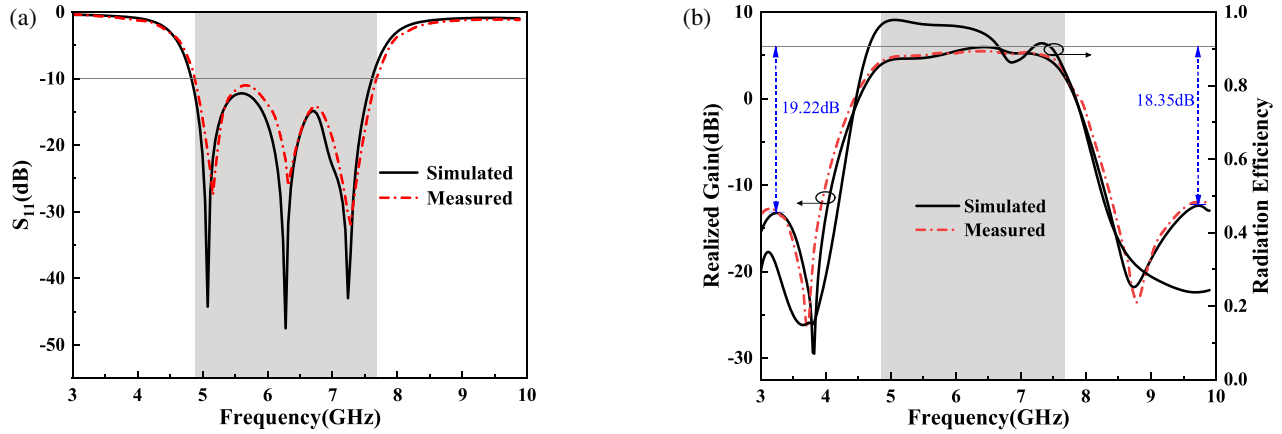

FIGURE 9. Simulated and measured S_{11}, realized gains, and radiation efficiencies of the filtering antenna. (a) S_{11}. (b) realized gains and radiation efficiency.

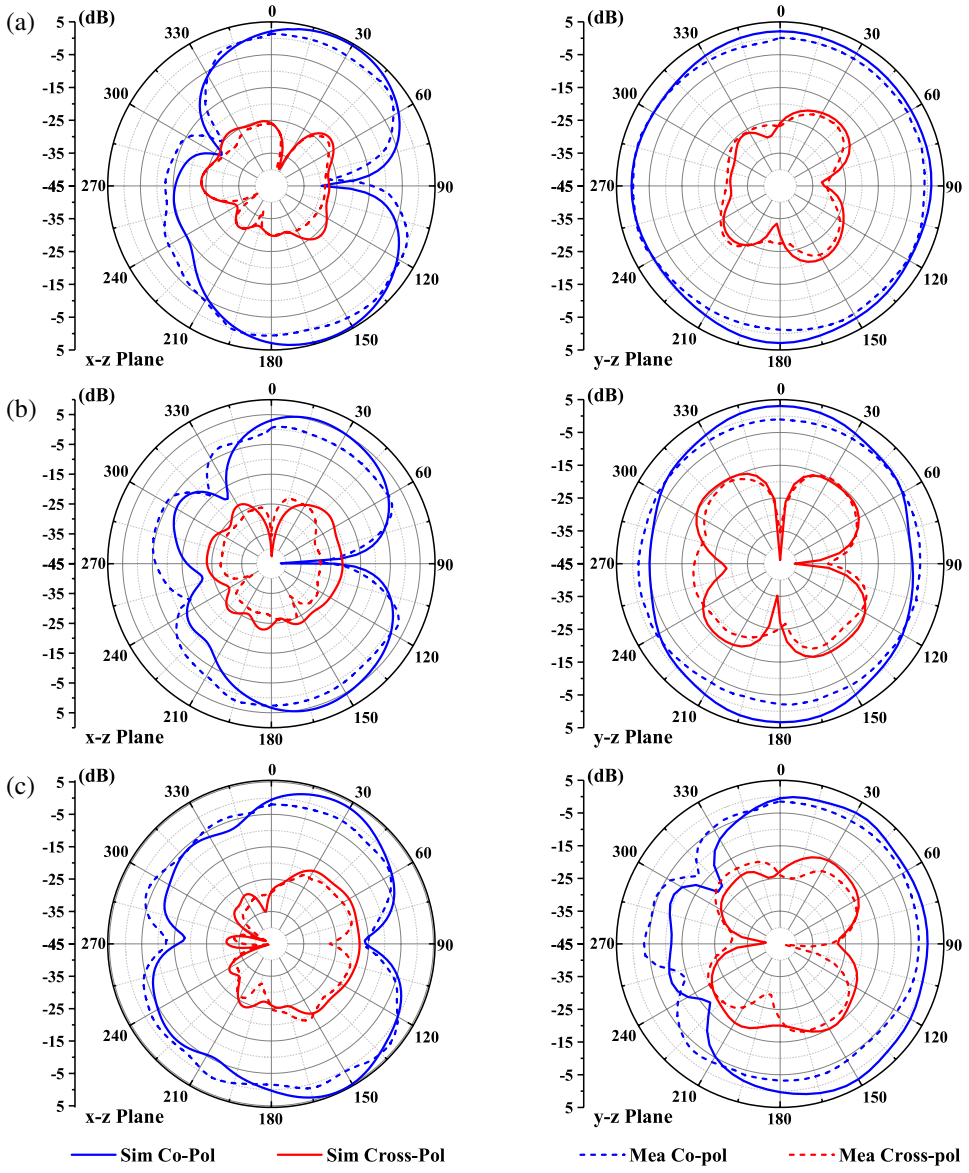

FIGURE 10. Simulated and measured radiation patterns of the filtering antenna in both xz and yz planes at different frequencies. (a) 5.08 GHz. (b) 6.28 GHz. (b) 7.26 GHz.

TABLE 2. Performance comparison of the filtering antennas.

Ref.	f_0 (GHz)	Size (mm ×mm) ($\lambda_0 \times \lambda_0$)	BW (%)	Gain (dBi)	Rejection level (dB)	F_L/F_U
[10]	1.8	113.2×113.2 (0.68×0.68)	27.8	6.5	19.0	0.63/0.30
[11]	2.05	70×50 (0.48×0.34)	33.8	4.1	12.1	0.12/0.20
[12]	11.8	18.5×13 (0.73×0.51)	11.84	5.0	6.5	0.98/0.20
[13]	5.24	40×33.8 (0.70×0.59)	7.0	6.6	13.0	0.68/0.76
[16]	4.98	25×25 (0.41×0.41)	21.5	4.8	15.9	0.33/0.44
[18]	2.84	66.5×50 (0.63×0.47)	9.2	5.75	11.0	0.19/0.20
[19]	2.0	68×68 (0.45×0.45)	7.0	5.6	19.6	0.88/0.50
This letter	6.22	35×29 (0.72×0.60)	44.6	5.7	18.2	0.25/0.22

points: 5.08 GHz, 6.28 GHz, and 7.26 GHz. It is evident that the antenna's radiation pattern remains stable across a wide frequency range, signifying its strong broadside radiation. Moreover, the simulated and measured radiation pattern results show good agreement at all three frequencies, with cross-polarization well maintained. The minor discrepancies between the simulated and measured results are primarily attributed to manufacturing tolerances and measurement conditions.

To highlight the advantages of the proposed antenna, Table 2 provides a comparison with other related filtering antennas in terms of bandwidth, size, gain, and frequency selectivity parameters. In the context of free space, λ represents the wavelength at f. The frequency rate selectivity of the lower and upper edges (F_L and F_U) of the passband is defined according to [18].

$$F_L = \frac{f_{10L} - f_{15L}}{f_{10U} - f_{10L}}, \quad F_U = \frac{f_{15U} - f_{10U}}{f_{10U} - f_{10L}} \tag{4}$$

where f_{10L} and f_{10U} are, respectively, the frequencies at which $S_{11} = -10$ dB at the lower and upper edges of the passband. f_{15L} and f_{15U} are the lower and upper frequencies corresponding to the 15 dB gain suppression values with respect to the gain at center frequency f_0, respectively. The smaller the values of F_L or F_U means the better frequency selectivity.

The table illustrates the advantages of the proposed filtering antenna, which include a small size, simple structure, flat profile, wide bandwidth, and high frequency selectivity. These characteristics align with the requirements for miniaturizing front-end devices. In comparison with alternative compact filtering antennas, the proposed antenna exhibits a superior operating bandwidth and enhanced out-of-band rejection capabilities, with an operating bandwidth of 44.6% and an out-of-band rejection level of 18.2 dB. Furthermore, in contrast to other antennas with additional filtering structures, its dimensions and fabrication process offer inherent advantages. The gain of the proposed antenna outperforms the antennas presented in [11, 12, 16]. While the gain is not particularly exceptional, it satisfies the fundamental requirements for the radiation performance of filtering antennas. The lower gain can be attributed to several factors, including the dimensions of the radiating patch and the high loss of the FR-4 substrate. The proposed antenna demonstrates superior frequency selectivity and a broader operating bandwidth compared to the filtering antennas in [10–13, 19]. Additionally, it exhibits better out-of-band rejection than the filtering antennas in [11, 12], 18]. While the gain of the proposed antenna is not exceptional, its overall performance is comparable to the average level of existing filtering antennas. Additionally, the proposed filtering antenna exhibits a wide bandwidth, high gain, high frequency selectivity, and excellent out-of-band rejection, all while meeting the requirements for miniaturization.

4. CONCLUSION

In this paper, a filtering antenna with wide bandwidth, high gain, high frequency selectivity, and high level of out-of-band rejection is designed. The incorporation of an asymmetric Y-shaped branch introduces two radiation nulls on either side of the antenna passband and appropriately broadens the bandwidth. Concurrently, the introduction of an L-shaped branch on the feedline further expands the impedance bandwidth of the antenna while enhancing its frequency selectivity and out-of-band rejection. This design achieves optimal in-band radiation performance and out-of-band frequency selectivity. The antenna achieves a balance between compact size (35 mm×29 mm×0.8 mm) and high gain without incorporating additional filtering structures. After fabricating and measuring the antenna prototype, the final design demonstrates excellent performance characteristics, including a wide operating bandwidth of 44.6% (4.88∼7.68 GHz), a peak realized gain of 5.7 dBi, a high out-of-band rejection level of 18.2 dB, and excellent frequency selectivity. Ultimately, the satisfactory radiation and filtering performance of the antenna make it suitable for applications in the 5G Sub-6 GHz and WiFi-6E bands.

ACKNOWLEDGEMENT

This work was supported in part the Natural Science Research Project of Anhui Educational Committee under grant No. 2022AH051583, No. 2022AH052138 and No. 2023AH052650, in part by the Anhui Province Graduate Academic Innovation Project under grant No. 2023xscx074, in part by the Funding Project of Scientific Research Starting for the High-level Talents of West Anhui University under grant No. WGKQ2022009.

REFERENCES

[1] Choudhary, D. K., N. Mishra, P. K. Singh, and A. Sharma, "Miniaturized power divider with triple-band filtering response using coupled line," *IEEE Access*, Vol. 11, 27 602–27 608, 2023.

[2] Mao, C.-X., S. Gao, Y. Wang, Q. Luo, and Q.-X. Chu, "A shared-aperture dual-band dual-polarized filtering-antenna-array with improved frequency response," *IEEE Transactions on Antennas and Propagation*, Vol. 65, No. 4, 1836–1844, Apr. 2017.

[3] Yu, C., W. Hong, Z. Kuai, and H. Wang, "Ku-band linearly polarized omnidirectional planar filtenna," *IEEE Antennas and Wireless Propagation Letters*, Vol. 11, 310–313, 2012.

[4] Mao, C.-X., S. Gao, Y. Wang, F. Qin, and Q.-X. Chu, "Multimode resonator-fed dual-polarized antenna array with enhanced bandwidth and selectivity," *IEEE Transactions on Antennas and Propagation*, Vol. 63, No. 12, 5492–5499, Dec. 2015.

[5] Qian, J.-F., F.-C. Chen, Y.-H. Ding, H.-T. Hu, and Q.-X. Chu, "A wide stopband filtering patch antenna and its application in MIMO system," *IEEE Transactions on Antennas and Propagation*, Vol. 67, No. 1, 654–658, Jan. 2019.

[6] Dhwaj, K., H. Tian, and T. Itoh, "Low-profile dual-band filtering antenna using common planar cavity," *IEEE Antennas and Wireless Propagation Letters*, Vol. 17, No. 6, 1081–1084, Jun. 2018.

[7] Chang, H., M. Liu, D. Lin, and J. Wang, "A compact single layer filtering antenna with DGS for 5.1 GHz application," *Progress In Electromagnetics Research Letters*, Vol. 107, 1–7, 2022.

[8] Choudhary, D. K. and R. K. Chaudhary, "Compact filtering antenna using asymmetric CPW-fed based CRLH structure," *AEU — International Journal of Electronics and Communications*, Vol. 126, 153462, Nov. 2020.

[9] Kukreja, J., D. K. Choudhary, and R. K. Chaudhary, "A short-ended compact metastructure antenna with interdigital capacitor and U-shaped strip," *Wireless Personal Communications*, Vol. 108, 2149–2158, May 2019.

[10] Xiang, B. J., S. Y. Zheng, Y. M. Pan, and Y. X. Li, "Wideband circularly polarized dielectric resonator antenna with bandpass filtering and wide harmonics suppression response," *IEEE Transactions on Antennas and Propagation*, Vol. 65, No. 4, 2096–2101, Apr. 2017.

[11] Chen, X., L. Zhu, and M. Li, "Design of wideband, compact, filtering slot antenna enabled with mixed electric/magnetic couplings," *IEEE Transactions on Antennas and Propagation*, Vol. 72, No. 4, 3718–3723, Apr. 2024.

[12] Yin, J.-Y., T.-L. Bai, J.-Y. Deng, J. Ren, D. Sun, Y. Zhang, and L.-X. Guo, "Wideband single-layer substrate integrated waveguide filtering antenna with U-shaped slots," *IEEE Antennas and Wireless Propagation Letters*, Vol. 20, No. 9, 1726–1730, Sep. 2021.

[13] Jin, J. Y., S. Liao, and Q. Xue, "Design of filtering-radiating patch antennas with tunable radiation nulls for high selectivity," *IEEE Transactions on Antennas and Propagation*, Vol. 66, No. 4, 2125–2130, Apr. 2018.

[14] Deng, J. and L. Feng, "Dual-band microstrip filtering antennas with symmetrical slots," *Progress In Electromagnetics Research Letters*, Vol. 86, 13–19, 2019.

[15] Li, L., H. D. Xiong, W. Y. Wu, A. B. Fu, and J. Y. Han, "A T-shaped strips loaded wideband filtering patch antenna with high selectivity," *IEEE Antennas and Wireless Propagation Letters*, Vol. 23, No. 1, 89–93, Jan. 2024.

[16] Chen, B.-J., X.-S. Yang, and B.-Z. Wang, "A compact high-selectivity wideband filtering antenna with multipath coupling structure," *IEEE Antennas and Wireless Propagation Letters*, Vol. 21, No. 8, 1654–1658, Aug. 2022.

[17] Yang, W.-J., Y.-M. Pan, and X.-Y. Zhang, "A single-layer low-profile circularly polarized filtering patch antenna," *IEEE Antennas and Wireless Propagation Letters*, Vol. 20, No. 4, 602–606, Apr. 2021.

[18] Hu, K.-Z., B.-C. Guo, S.-Y. Pan, D. Yan, M.-C. Tang, and P. Wang, "Low-profile single-layer half-mode SIW filtering antenna with shorted parasitic patch and defected ground structure," *IEEE Transactions on Circuits and Systems II: Express Briefs*, Vol. 70, No. 1, 91–95, Jan. 2023.

[19] Tang, M.-C., D. Li, Y. Wang, K.-Z. Hu, and R. W. Ziolkowski, "Compact, low-profile, linearly and circularly polarized filtennas enabled with custom-designed feed-probe structures," *IEEE Transactions on Antennas and Propagation*, Vol. 68, No. 7, 5247–5256, Jul. 2020.

[20] Zhang, X. Y., W. Duan, and Y.-M. Pan, "High-gain filtering patch antenna without extra circuit," *IEEE Transactions on Antennas and Propagation*, Vol. 63, No. 12, 5883–5888, Dec. 2015.

[21] Xu, K., J. Shi, X. Qing, and Z. N. Chen, "A substrate integrated cavity backed filtering slot antenna stacked with a patch for frequency selectivity enhancement," *IEEE Antennas and Wireless Propagation Letters*, Vol. 17, No. 10, 1910–1914, Oct. 2018.

[22] Yang, W., S. Chen, Q. Xue, W. Che, G. Shen, and W. Feng, "Novel filtering method based on metasurface antenna and its application for wideband high-gain filtering antenna with low profile," *IEEE Transactions on Antennas and Propagation*, Vol. 67, No. 3, 1535–1544, Mar. 2019.

[23] Cheng, G., J. Zhou, B. Huang, L. Yang, and Z. Huang, "Compact low-profile wideband filtering antenna without additional filtering structure," *IEEE Antennas and Wireless Propagation Letters*, Vol. 22, No. 10, 2477–2481, Oct. 2023.

[24] Chen, X., Q. Zhuge, G. Han, R. Ma, J. Su, and W. Zhang, "A wideband harmonic suppression filtering antenna with multiple radiation nulls," *Progress In Electromagnetics Research Letters*, Vol. 112, 17–25, 2023.

[25] Pan, Y. M., P. F. Hu, X. Y. Zhang, and S. Y. Zheng, "A low-profile high-gain and wideband filtering antenna with metasurface," *IEEE Transactions on Antennas and Propagation*, Vol. 64, No. 5, 2010–2016, May 2016.

[26] Yang, W., J. Huang, D. Chen, K.-l. Yu, Q. Xue, and W. Che, "Broadband dual-polarized filtering metasurface-based antennas using characteristic mode analysis for 5G millimeter-wave applications," *IEEE Transactions on Antennas and Propagation*, Vol. 72, No. 5, 3912–3927, May 2024.

[27] Yuan, H., F.-C. Chen, and Q.-X. Chu, "A wideband and high gain dual-polarized filtering antenna based on multiple patches," *IEEE Transactions on Antennas and Propagation*, Vol. 70, No. 10, 9843–9848, Oct. 2022.

[28] Cheng, G., B. Huang, Z. Huang, and L. Yang, "A high-gain circularly polarized filtering stacked patch antenna," *IEEE Antennas and Wireless Propagation Letters*, Vol. 22, No. 5, 995–999, May 2023.

[29] Liang, G.-Z., F.-C. Chen, H. Yuan, K.-R. Xiang, and Q.-X. Chu, "A high selectivity and high efficiency filtering antenna with controllable radiation nulls based on stacked patches," *IEEE Transactions on Antennas and Propagation*, Vol. 70, No. 1, 708–713, Jan. 2022.

[30] Leonardi, O., M. G. Pavone, G. Sorbello, A. F. Morabito, and T. Isernia, "Compact single-layer circularly polarized antenna for short-range communication systems," *Microwave and Optical Technology Letters*, Vol. 56, No. 8, 1843–1846, May 2014.